# Investigation of Amorphous Oxide Film-Electrolyte Junctions by AC Techniques

**S. Piazza, C. Sunseri, and F. Di Quarto**
Dipartimento di Ingegneria Chimica dei Processi e dei Materiali, Università degli Studi di Palermo, Viale delle Scienze, 90128 Palermo, Italy

*Current AC (alternating current) techniques are used often to characterize the energetics at a semiconducting solid phase/electrolyte interface. For thin layers having a strongly disordered or amorphous structure (such as oxide-passive layers anodically grown on valve metals), interpretative models currently used for crystalline semiconductors may produce misleading data.*

*A new interpretation of the admittance data, based on recent models for amorphous semiconductors (a-Sc) Schottky barriers, is presented for passive films of Nb, W and Ti. The physical bases of the model are presented as well as its advantages and disadvantages. The new theory views the solid/electrolyte interface more satisfactorily and provides information on the solid-state properties and the electronic structure of the electrode useful for interpreting the electron exchange between the solid phase and redox couples in solution.*

## Introduction

Interest in the semiconductor/electrolyte interface has been increasing in the past decade due to its potential application to solar energy conversion (Gerischer, 1979). The materials investigated for this purpose were essentially single crystal semiconductors (SC) having a relatively low band gap (1 ÷ 2 eV) and good transport properties of the photogenerated carriers (Heller, 1982).

Some recent investigations focused on the junction formed between a thin surface film grown on a metal (for example, an oxide) and an electrolytic solution (Stimming, 1986; Burleigh, 1989). Knowledge of the energetics of this interface is an important task in the fields of photoelectrochemistry and corrosion (Gerischer, 1990). In fact, it is widely accepted that the resistance of the base metal to the corrosive attack by the environment depends greatly on the solid-state properties of these surface films (Sato, 1989). In this case, however, the solid phases are often amorphous or strongly disordered. This fact introduces some differences with respect to the case of crystalline SC.

To get information on the mechanisms of charge transfer at the interface, one must know the location of the characteristic energy levels of the solid, like the conduction (C.B.) and the valence (V.B.) band edges, and the Fermi level ($E_F$). For this information, AC techniques are often used, which permit recording the so-called differential capacitance of the interface as a function of the electrode potential.

For single crystal SC, the Mott-Schottky (M-S) theory (see, for example, Pleskov and Gurevich, 1986) predicts an inverse relationship between the square of the space charge capacity of the SC ($C_{sc}$) and the band bending (the electrode potential), according to the formula:

$$\frac{1}{C_{sc}^2}=\frac{2}{\epsilon\epsilon_0|e|N_d}\left(U_E-U_{FB}+\frac{kT}{|e|}\right) \tag{1}$$

where $\epsilon$ is the relative dielectric constant of the solid, $\epsilon_0$ the vacuum permittivity, $N_d$ the concentration of ionized donors (for $n$-type SCs), $U_E$ the electrode potential, and $U_{FB}$ the flat band potential, that is, the characteristic potential of the junction where the bands are flat throughout the solid. The last quantity is related to the Fermi level of the SC by the relationship:

$$E_F=-|e|U_{FB}$$

Based on this theory, $C_{sc}^{-2}$ vs. $U_E$ plots have been used widely in the literature to get the energetics of the SC/electrolyte junction.

In the frame of the M-S theory, no frequency dependence of $C_{sc}$ is foreseen. When a frequency dispersion of the experimental capacitance was observed, the presence of surface states at the interface or midgap states has been invoked to explain the experimental results (Roberts and Crowell, 1970; Losee, 1975; Gomes and Cardon, 1982; Fonash, 1983; Bonham and Orazem, 1988).

For amorphous oxide films grown anodically on valve metals, a systematic dependence of the measured capacity on the frequency of the AC signal has been observed (Di Quarto et al., 1990, 1991). This behavior can hardly be justified according to the theory of single crystal SC, and it has been attributed to the amorphous structure of the semiconducting films. In these cases, the use of the M-S plots for detecting the energy levels at the interface leads to inconsistency of the results (Di Quarto et al., 1990). In fact, the change of solid-state properties with respect to the case of crystalline materials is so sharp that the hypotheses underlying the M-S theory are no longer valid, so that one must reconsider the physical picture of the interface.

## Physical Model of the Interface and AC Response

Amorphous or strongly disordered materials are characterized by a distribution of localized electronic states lying within the forbidden energy region (Cohen et al., 1969; Mott and Davis, 1979). The origin of these electronic states lies in the lack of long-range order in such materials. At variance with the case of crystalline SC, electrical conduction is possible through such states. Because in these states there is only a partial overlapping of the electronic wave functions between adjacent sites, conduction in localized gap states occurs mainly by a hopping mechanism. As a consequence, there is a drop in the carrier mobility when passing from the energy region of the extended states to that of the localized ones (Mott and Davis, 1979). This sharp variation of mobility can be used to locate the C.B. and V.B. mobility edges of the amorphous semiconductor (a-SC).

The presence of a continuous distribution of states (DOS) within the mobility gap of the a-SC has a great influence on the overall behavior of the material, which differs in many aspects from that of the single crystal SCs. In particular, it affects noticeably the AC response of the a-SC/electrolyte junction. In fact, localized states contribute to the total space charge of the a-SC, so that the Poisson equation must be now modified to include this term. For $n$-type semiconductors, the positive space charge density is given by (Spear and Baker, 1989):

$$\rho^{+} = |e| N_d + \rho_L \tag{2}$$

where $\rho_L$ represents the contribution of localized states at each point of the junction for each polarization. At zero frequency, it is usually assumed that all states attain their thermal equilibrium occupation, while under AC polarization the response coming from localized states depends both on their energy and on the angular frequency of the signal, $\omega$, due to the finite response time of the deep-lying electronic states. Hence, the measured differential capacitance of the barrier will depend on how fast localized states can respond to the AC perturbation by changing their occupation.

It is usually assumed (Abram et al., 1982; Cohen et al., 1982) that the time constant for the capture (or emission) of carriers into (from) a localized state is given by:

$$\tau = \tau_0 \exp\left(\frac{E_c - E}{kT}\right) \tag{3}$$

where $E$ is the energy of the localized state, and $E_c$ the C.B. mobility edge. In Eq. 3, $\tau_0$ is a constant characteristic for each material.

Equation 3 indicates that by decreasing the energy of the state in the gap of the a-SC, $\tau$ increases sharply so that deep states do not respond to the AC signal any more as long as the condition, $\omega\tau \gg 1$, is fulfilled.

A simplified treatment of the a-SC/electrolyte junction has been reported (Di Quarto et al., 1986, 1990) analogously to the theoretical model proposed for solid-state a-SC Schottky barrier (Abram et al., 1982; Cohen et al., 1982). The model assumes a sharp cutoff energy level, $E_\omega$, which separates states that fully respond to the AC perturbation from those giving a null response. The energy position of $E_\omega$ at each frequency can be found by imposing the condition $\omega\tau = 1$ in Eq. 3.

The physical situation is shown in Figure 1. The intersection of $E_\omega$ with the Fermi level separates the solid in two regions: the region for $x < x_c$ (region of null response for the localized states), which behaves like a pure dielectric and the full response region for $x > x_c$. Thus, the total capacitance of the space charge region of the a-SC can be seen as the sum of two capacitors in series (Figure 2), of which one, $(\epsilon\epsilon_0/x_c)$, depends on frequency, while the other, $[C(\psi_c,0)]$, does not. Moreover, it has been shown that the conductance of the barrier arises mainly from the region near $x_c$ (Cohen et al., 1982; Archibald et al., 1983). Thus, the equivalent circuit of the barrier is shown in Figure 2, where the Helmholtz capacity in the electrolyte side of the junction has been considered.

For spatially homogeneous materials having a constant DOS,

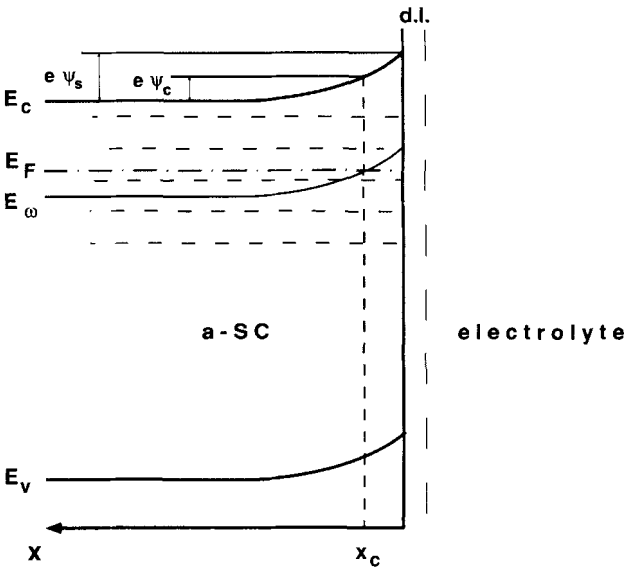


**Figure 1. Energetics at an amorphous SC/electrolyte junction.**

$E_c$ and $E_v$ are the mobility edges, and $E_F$ the Fermi level. Dashes represent localized electronic states. The double layer (d.l.) in the solution side of the junction is also reported.

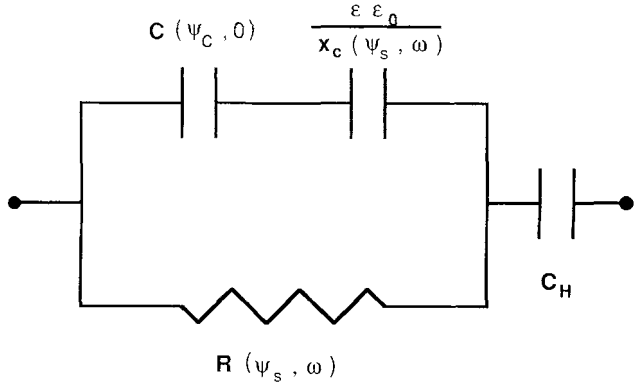


**Figure 2. Equivalent electrical circuit for interpreting impedance data on the a-SC/electrolyte junction.**

$N$, within the mobility gap, the capacity and conductance of the space charge region are given (Archibald and Abram, 1983) by:

$$C(\psi_s,\omega)=\frac{(\epsilon\epsilon_0|e|^2N)^{1/2}}{1+\ln(\psi_s/\psi_c)} \tag{4}$$

$$G(\psi_s,\omega)=\frac{\omega\pi}{2}\frac{kT}{|e|\psi_c}\frac{(\epsilon\epsilon_0|e|^2N)^{1/2}}{[1+\ln(\psi_s/\psi_c)]^2} \tag{5}$$

In Eqs. 4 and 5, $\omega$ is the angular frequency of the AC signal, $\psi_s=U_E-U_{FB}$ the band bending and $\psi_c$ the band bending at $x_c$ (see Figure 1) given by:

$$|e|\psi_c=-kT\ln(\omega\tau_0)-\Delta E_F \tag{6}$$

with $\Delta E_F=(E_c-E_F)$ bulk.

It is important to note that Eqs. 4–6 are only approximate for a nonconstant DOS; however, they can be applied for a DOS slowly varying with the energy (Cohen and Lang, 1982; Archibald and Abram, 1983).

Equations 4–5 contain the frequency dependence of both components of the space charge region admittance through $\psi_c$ and $\omega$. In a recent article by Dean and Stimming (1989), an expression for the zero-frequency capacitance has been used for interpreting experimental data obtained at 1 kHz. It has been shown by Abram et al. (1982) and Snell et al. (1980) that neglecting the frequency effect on the capacitance vs. potential curve gives rise to serious errors. In the absence of an impedance study of the junction at different frequencies, the DOS distribution postulated by Dean and Stimming (1989) must be regarded as an *ad hoc* assumption.

## Results and Discussion

### *Fitting the experimental curves*

Figure 3 shows the curves of the measured parallel capacitance of the interface, $C_m$, vs. the electrode potential, $U_E$, at different frequencies for an a-$WO_3$ film grown anodically in 0.5-M $H_2SO_4$ solution up to a thickness of about 54 nm. Such curves have been obtained using the lock-in technique in the anodic polarization region where a blocking behavior of the

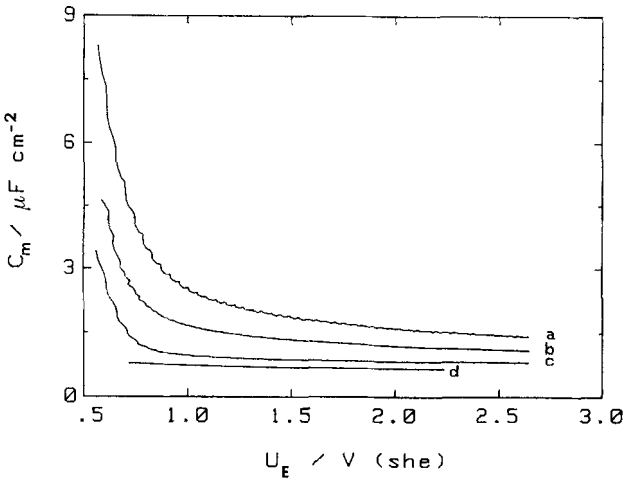


**Figure 3. Measured parallel capacitance, $C_m$, vs. electrode potential at different frequencies in 0.5-M $H_2SO_4$ solution for an a-$WO_3$ film grown up to 54 nm.**

***a) f = 3 Hz; b) f = 10 Hz; c) f = 100 Hz; d) f = 3 kHz.***

interface is observed. With this method, a small (≤20-mV peak-peak) AC signal is superimposed to the linear potential sweep, and the components of the overall impedance are derived from the in-phase and out-of-phase components of the AC current circulating. The curves at lower frequencies display a sharp increase of the capacity at low potentials near the flat band potential of the film. At high frequencies, the capacitance curves tend to flatten. This behavior has been observed also with anodic films of a-$Nb_2O_5$ (Di Quarto et al., 1990) and a-$TiO_2$ in contact with different electrolytes.

The behavior depicted in Figure 3 is consistent with the prediction of the model outlined in the previous section, if we take into account that by increasing the frequency $E_\omega$ shifts upwards in the mobility gap of the a-SC. Thus, the region of null response widens, and at sufficiently high frequency all the film behaves as a pure dielectric giving a nearly constant capacitance.

It is worth noting that the use of M-S plots for this case should give ambiguous results, as shown in Figure 4 for the a-$WO_3$ film of Figure 3, where the initial region of the $C_{sc}^{-2}$ vs. potential plots presents a nearly linear behavior, but both the slope and the intercept of the straight lines depend strongly on the frequency of the AC signal. At high frequency, the latter shifts toward unreasonably negative values and tends to $-\infty$. Hence, this type of analysis does not allow a clear determination of the $N_d$ as well as the $U_{FB}$ values.

Another important aspect of the results of Figure 3 is that the final value of the capacitance at high anodic electrode potentials also depends on frequency. At very high frequency, it tends to a limiting value given by the geometrical capacitance of the oxide:

$$C_{ox}=\frac{\epsilon\epsilon_0}{d} \tag{7}$$

where $d$ is the oxide thickness. This finding is shown in Figure 5 for different a-$WO_3$ films grown in 1-M $H_3PO_4$ solution: the

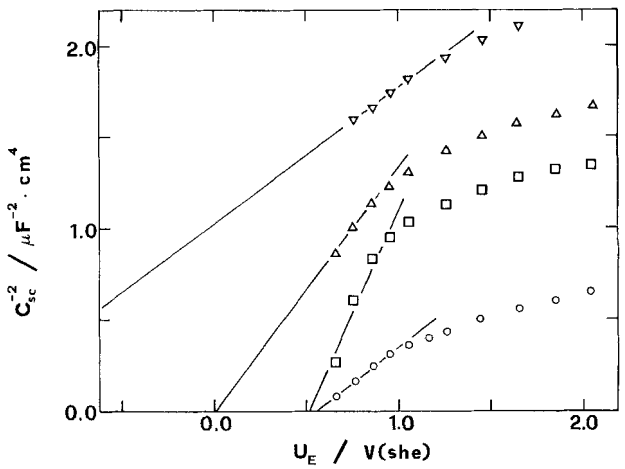


**Figure 4. Mott-Schottky plots at different frequencies for the a-$WO_3$ film of Figure 3.**

o, $f$ = 10 Hz; □, $f$ = 100 Hz; △, $f$ = 1 kHz; ▽, $f$ = 3 kHz.

$1/C_{ox}$ vs. the formation voltage ($V_F$, equal to the anodizing ratio times the oxide thickness) plot recorded at 10 kHz is linear according to Eq. 7. From the slope of the straight line of Figure 5, a value of $\epsilon \cong 45$ is derived for the film, which is in agreement with the literature data (Di Quarto et al., 1980). An initial film thickness before anodization $d_0 \cong 3$ nm can be inferred from the data in Figure 5. Such a behavior is also consistent with the model of a-SC/electrolyte interface.

The in-phase component of the measured admittance also strongly depends on the frequency. This is shown in Figure 6 for the a-$WO_3$ film of Figures 3-4. However, the flattening of the $G_m$ curves with increasing frequency is far more gradual than that of the capacitance curves. In both cases, the curves flatten at lower frequency for thicker films (Di Quarto et al., 1990, 1991).

To fit the experimental curves according to Eqs. 3-4, one must convert the components of the parallel equivalent admittance, $C_m$ and $G_m$, measured with the lock-in technique into the space charge region capacitance and conductance, $C_{sc}$ and $G_{sc}$, according to the equivalent circuit depicted in Figure 2. This has been done numerically using a computer program according to the following formulas:

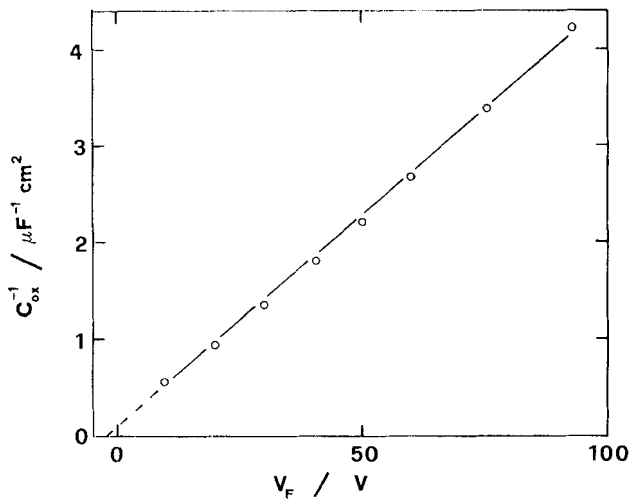


**Figure 5. Reciprocal oxide capacitance vs. formation voltage, $V_F$, for a-$WO_3$ films grown in 1-M $H_3PO_4$ solution at 4 mA·cm².**

Anodizing ratio, 1.75 nm/V; measuring frequency, $f$ = 10 kHz.

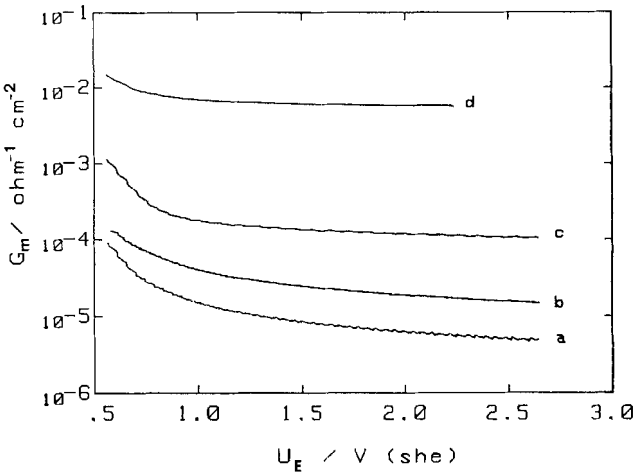


**Figure 6. Measured parallel conductance, $G_m$, vs. electrode potential at different frequencies in 0.5-M $H_2SO_4$ solution for an a-$WO_3$ film grown up to 54 nm.**

*a) $f$ = 3 Hz; b) $f$ = 10 Hz; c) $f$ = 100 Hz; d) $f$ = 3 kHz.*

$$\tilde{Y}_m = \frac{1}{\tilde{Z}_{sc} + \tilde{Z}_H} \tag{8a}$$

$$\tilde{Y}_m = |Y_m| e^{j\varphi_m} \tag{8b}$$

$$|Y_m| = \sqrt{G_m^2 + \omega^2 C_m^2} \tag{8c}$$

$$\varphi_m = \text{arctg}\left(\frac{\omega C_m}{G_m}\right) \tag{8d}$$

where $\tilde{Y}_m$ is the complex parallel admittance measured having $\varphi_m$ as the phase angle, $\tilde{Z}_{sc}$ and $\tilde{Z}_H$ are the complex impedances arising from the space charge region of the a-SC and from the electrolyte double-layer, respectively.

The fitting procedure was carried out on both components of $\tilde{Y}_{sc} = \tilde{Z}_{sc}^{-1}$ by imposing the condition that all curves relative to the same specimen must give the same $U_{FB}$ value within the experimental precision, regardless of the frequency. Moreover, additional costraints were imposed on the $\psi_c$ values derived from the fitting procedure, which should be equal for both components at the same frequency and change of approximately 59 mV for decade of frequency, as theoretically foreseen (see Eq. 6).

We have to say that all these conditions were not always fulfilled simultaneously. Moreover, we observed deviations from the standard behavior for some samples oxidized in apparently identical conditions. This finding raises the question of the microscopic control of the anodization procedure and

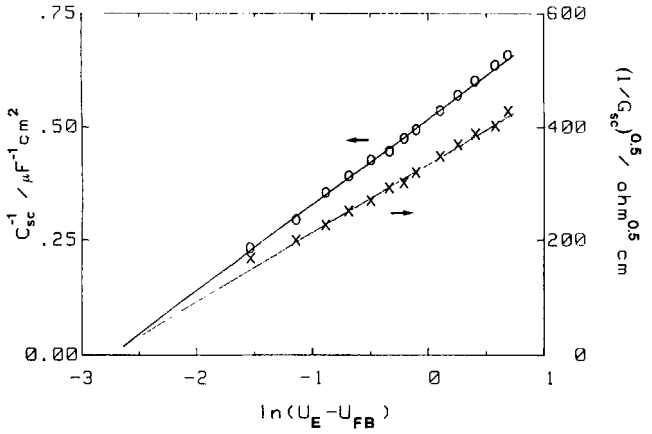


**Figure 7. Fitting of impedance data at $f = 3$ Hz for the a-$WO_3$ film of Figures 3 and 6.**

Straight lines are the theoretical curves obtained according to Eqs. 4-5. Symbols are the "experimental" $C_{sc}$ and $G_{sc}$ values obtained after correction for the equivalent circuit of Figure 2.

its influence on the solid-state properties of the amorphous anodic films (Di Quarto et al., 1987b, 1990). However, for the great majority of the samples examined, the above conditions were satisfied when varying the $U_{FB}$ value within $\pm 50$ mV.

Figure 7 shows the fitting of the capacitance and conductance curves at $f = 3$ Hz for the a-$WO_3$ film of Figures 3 and 6. Symbols represent the values of $C_{sc}$ and $G_{sc}$ obtained from the measured quantities after correction according to formulas 8a-8d. An excellent agreement with the straight lines theoretically predicted by Eqs. 4-5 is observed in a quite large potential interval. In other cases, the linear region of the experimental plot is smaller, but always larger than about 0.8 V. From the fitting procedure, it is possible to derive the solid-state parameters for the investigated film. The variation of $\psi_c$ with the frequency is reported in Figure 8 for three different oxide films in the realm of validity of Eqs. 4-5 for $\psi_s > \psi_c \geq 3\ kT/|e|$ (Archibald and Abram, 1983).

### *Frequency dispersion of the conductance and DOS profile*

Table 1 shows the results obtained with different oxides in

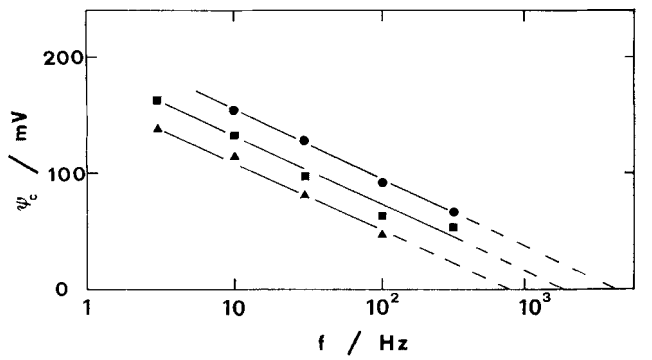


**Figure 8. $\psi_c$ value as a function of frequency for three anodic films grown in 0.5-M $H_2SO_4$ solution.**

▲, 89-nm-thick a-$WO_3$; ■, 83-nm-thick a-$TiO_2$; ●, 84-nm-thick a-$Nb_2O_5$.

**Table 1. Physical Parameters for Three Anodic Oxide Films from the Fitting, According to Eqs. 4-5, of the Impedance Data in 0.5-M $H_2SO_4$***

| Oxide | Thickness nm | $U_{FB}$ V(SHE) | $\psi_c(f=3$ Hz) mV | $\Delta E_F$ eV | $N(E_F)$ $cm^{-3} \cdot eV^{-1}$ |
|---|---|---|---|---|---|
| a-$WO_3$ | 54 | $0.51 \pm 0.04$ | 174 | 0.44 | $2.0 \times 10^{19}$ |
| a-$Nb_2O_5$ | 84 | $0.06 \pm 0.04$ | 186 | 0.43 | $1.5 \times 10^{19}$ |
| a-$TiO_2$ | 83 | $0.10 \pm 0.05$ | 162 | 0.45 | $2.3 \times 10^{20}$ |

*After correction for the electrical equivalent circuit of Figure 2, a value of 30 $\mu F \cdot cm^{-2}$ has been used for $C_H$.

0.5-M $H_2SO_4$ solution. A value of 30 $\mu F \cdot cm^{-2}$ was assumed for $C_H$ in all cases. It is worth mentioning that the values of the average DOS, $N$, in the table are taken from the fitting of the $C_{sc}$ curves on the basis of the relative dielectric constant reported in the literature for each oxide. In fact, the $\epsilon N$ values derived from the fitting of the $G_{sc}$ vs. potential curves show a larger frequency dispersion. This fact must be attributed to the spectroscopic character of the conductance plots, which are sensitive to the real DOS profile within the mobility gap of the oxide, at variance with the capacitance curves. This implies that a reliable average value of the DOS in the energy region investigated can be extracted only from the latter curves, as experimentally verified.

The spectroscopic character of the conductance curves allows an estimation of the DOS profile within the mobility gap of the oxide films, making use of the formula proposed by Archibald and Abram (1986):

$$N[E_F - |e|\psi_c(\omega)] \cong KG/\omega \tag{9}$$

where $K$ is a constant approximately independent of frequency. An estimate of $K$ in the potential region where leakage current is small can be obtained from the average $N$ value derived at intermediate frequency from the fitting of the capacitance curve (see Table 1). This procedure has been proved to give a good fitting of the DOS distribution for a-Si solid-state Schottky barriers (Archibald and Abram, 1986).

Examples of application of Eq. 9 are reported in Figures 9-10 which are relative to a 54-nm-thick a-$WO_3$ film and to a 83-nm-thick a-$TiO_2$ layer in the same solution. A different behavior can be observed in both cases leading to slightly different DOS profiles. In fact, in the former case, the variation of $G_{sc}/\omega$ with the frequency indicates a nonconstant DOS profile in the vicinity of the Fermi level (see Figure 11a), while in the latter case, the almost constant value of $G_{sc}/\omega$ implies a nearly constant DOS in the explored region (Figure 11b). For a-$Nb_2O_5$ anodic films in 0.5-M $H_2SO_4$ solution, a behavior similar to that depicted in Figure 11a has been reported by Di Quarto et al. (1990).

Interestingly, the distribution of states reported in Figure 11a for the a-$WO_3$ film grown in sulfuric acid solution differs slightly from that detected in acetonitrile for a-$WO_3$ films grown in $H_3PO_4$ electrolyte (Di Quarto et al., 1991). This confirms the effect of the anodizing electrolyte on the solid-state properties of passive layers; in particular, the incorporation of phosphate and sulfate ions could influence in a different way the distribution of localized states within the mobility gap of the film. Further research on this aspect seems to be necessary.

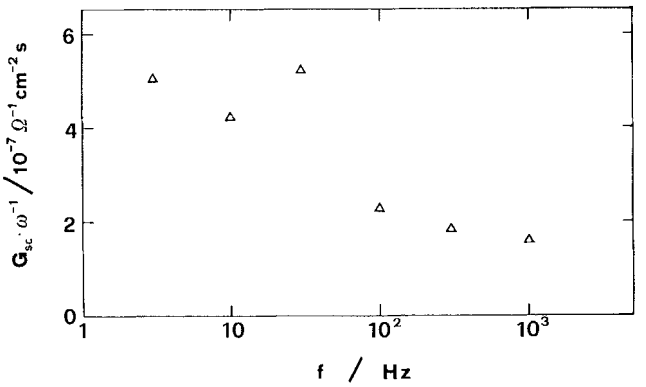


**Figure 9. $G_{sc}/\omega$ vs. frequency for a 54-nm-thick a-$WO_3$ film in 0.5-M $H_2SO_4$ solution.**

Band bending: $\psi_s = 1$ V.

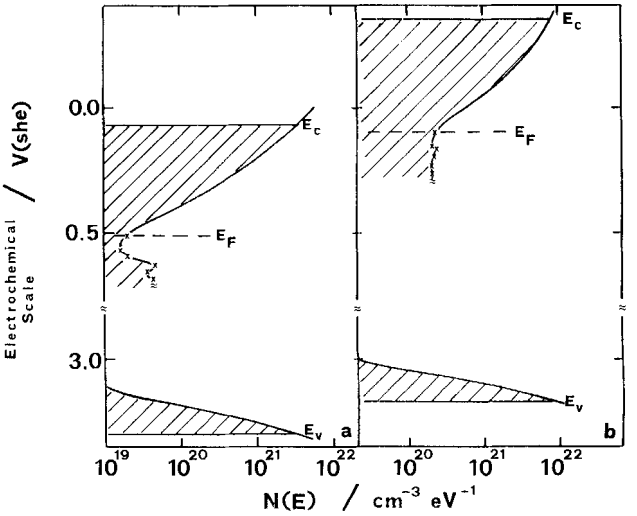


**Figure 11. Energy levels (electrochemical scale) at the oxide/0.5-M $H_2SO_4$ interface and DOS distribution in the vicinity of the Fermi level for the anodic oxide films of Figures 9-10.**

***a) 54-nm-thick a-$WO_3$; b) 83-nm-thick a-$TiO_2$.***

Symbols are the DOS values calculated according to Eq. 9. $E_c - E_v$ is the mobility gap; dashed regions are localized states.

We remark that the DOS profiles in Figure 11 are approximate due to the rough validity of Eq. 9. Moreover, because of the frequency limitation coming from the technique used for analyzing the interface, the investigated region of energy around $E_F$ is necessarily small. In fact, the practical range of frequency accessible with the lock-in technique is limited to $3 \div 5$ Hz in the lower domain. This means that in all cases pertaining to this work the investigated energy region is within about 200 meV around the Fermi level.

An improved setup could extend this range to some hundreds of millielectronvolts; nevertheless, considering that the exploration of the region placed 1 eV below $E_F$ requires a frequency of the order of $10^{-10}$ Hz, we can rule out the possibility of obtaining information on the DOS profile in a large part of the mobility gap of the oxides by using admittance techniques.

### *Location of the energy levels at the interface*

The results presented in the previous sections allow some considerations on the location of the characteristic energy levels of the oxide phase at the interface.

First of all, we note that the physical picture derived on the basis of the new model adopted differs markedly from that proposed by many authors in the literature based on the M-S approach. The location of the C.B. mobility edge, $E_c$, can be found by means of Eq. 6, after determining the flat band potential and the value of $|e|\psi_c$ at some frequency.

However, an uncertainty still remains due to the fact that the value of $\tau_0$ is not known *a priori*. This parameter can be related to the capture cross-section of the localized states and depends on the number and type of electronic defects in each disordered material. In the frame of the theory of a-SC Schottky barriers, $\tau_0$ is assumed to be an adjustable parameter, with the only assumption that Eq. 3 is able to describe the energy dependence of the relaxation time for the emission process from a localized gap state into the conduction band. Values of $\tau_0$ ranging between $10^{-10}$ and $10^{-14}$ s are reported in the literature for different materials (Losee, 1975; Abram and Doherty, 1982).

To derive reliable values for $\Delta E_F$ in Table 1, we used $\tau_0 = 10^{-12}$ s as a mean value for all the oxides. Using this figure it has been possible to locate the C.B. mobility edge of the different oxide films, as reported in Figures 11a-11b for the films of Figures 9-10 in contact with a 0.5-M $H_2SO_4$ electrolyte where the symbols are the values of density of states near the Fermi level calculated with the aid of Eq. 9. In Figure 11, optical band gap values equal to $3.05 \pm 0.05$ eV and $3.35 \pm 0.1$ eV have been assumed for the a-$WO_3$ film and the a-$TiO_2$ film, respectively, according to our own photoelectrochemical data. Moreover, a small tail of localized states in the vicinity of the V.B. mobility edge has been supposed to be present due to the disordered structure of the film, as foreseen by the theory of amorphous materials (Mott and Davis, 1979).

On the basis of the previous considerations, it follows that the position of the mobility edges derived results in an uncertainty of about $\pm 150$ meV.

In spite of this indetermination, it is possible to stress some important differences between the present case and that of a single crystal SC/electrolyte junction.

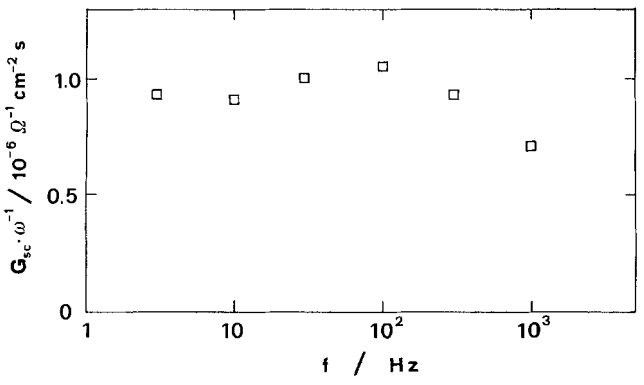


**Figure 10. $G_{sc}/\omega$ vs. frequency for a 83-nm-thick a-$TiO_2$ film in 0.5-M $H_2SO_4$ solution.**

Band bending: $\psi_s = 1$ V.

• The Fermi level is quite deeper in the forbidden gap with respect to the results obtainable from the theory of crystalline SCs. In this case, $E_c$ is usually placed by using the formula:

$$E_c = E_F + kT/|e| \ln(N_c/N_d) \tag{10}$$

where $N_c$ is the effective density of states at the bottom of the C.B. ($\geq 10^{20}$ cm$^{-3}$) and $N_d$ is the apparent donor density derived from the M-S plots with the aid of Eq. 1. Common values of $N_d$ reported for these systems are of the order of $10^{19}$ cm$^{-3}$, leading to $E_c - E_F \leq 0.1$ eV. From Table 1, it can be inferred that in any case $E_F$ is placed at least $\sim 0.4$ eV below $E_c$. This is another source of error when using the theory valid for crystalline SCs to characterize the a-SC/electrolyte junction.

• The presence of a continuous distribution of localized states in the region around $E_F$ affects the kinetics of electron exchange with the electrolyte. In fact, these states can take part in the electron transfer from/to the solution; in this case, the transfer kinetics becomes a function of the DOS distribution and the localization degree of the gap states. This leads to a different behavior with respect to the case of electron exchange with a single crystal SC, as reported for the kinetics of oxidation of $Fe^{2+}$ ions at a-$WO_3$ anodic films (Di Quarto et al., 1991).

## Conclusions

The systematic investigation of the metal/oxide/electrolyte junction for different anodic films on valve metals has shown a remarkable dependence of the barrier admittance on the frequency of the AC signal. This finding has been associated with the amorphous or strongly disordered structure of such films, which induces the presence of electronic localized states within the forbidden energy region. These states affect also the photoelectrochemical behavior of the junction (Di Quarto et al., 1987a,b).

To account for the observed behavior, reference has been made to a model for a-SC Schottky barriers proposed by Abram et al. (1982), Cohen and Lang (1982), and Archibald and Abram (1983). The fitting of the experimental data has allowed the determination of reliable values of the flat band potential for the different oxides and an estimation of the distribution of states close to the Fermi level.

This work has pointed out the inadequacy of models valid for single crystal semiconductors to rationalize the behavior of the investigated systems. This can help explain some inconsistencies often encountered in the current literature when dealing with the energetics of an anodic oxide/electrolyte junction.


## Acknowledgment

The authors are grateful to Dr. V. O. Aimiuwu (University of Benin) for performing some experiments.


## Notation

$C_m$ = experimentally measured capacitance of the solid/electrolyte interface, F/m$^2$
$C_{sc}$ = semiconductor space charge capacitance, F/m$^2$
$C_{ox}$ = oxide geometrical capacitance, F/m$^2$
$d$ = oxide thickness, m
$e$ = electron charge, C
$E$ = energy of the localized state, eV
$E_c$ = conduction band mobility edge, eV
$E_F$ = Fermi level of the solid phase, eV
$E_v$ = valence band mobility edge, eV
$E_\omega$ = cutoff level, eV
$f$ = frequency, Hz
$G_m$ = experimentally measured conductance of the solid/electrolyte interface, $\Omega^{-1}\cdot$m$^{-2}$
$G_{sc}$ = semiconductor space charge conductance, $\Omega^{-1}\cdot$m$^{-2}$
$j$ = $\sqrt{-1}$
$k$ = Boltzman's constant, $8.62\times10^{-5}$ eV/K
$N(E)$ = density of states, M
$N_d$ = ionized donor concentration, M
$N_c$ = effective density of conduction band states, M
$T$ = absolute temperature, K
$U_E$ = electrode potential, V
$U_{FB}$ = flat band potential, V
$V_F$ = formation voltage, V
$x$ = distance from the interface within the solid phase, m
$x_c$ = characteristic distance for the cutoff, m
$\tilde{Y}_m$ = measured complex admittance, $\Omega^{-1}\cdot$m$^{-2}$
$\tilde{Y}_{sc}$ = semiconductor space charge complex admittance, $\Omega^{-1}\cdot$m$^{-2}$
$\tilde{Z}_{sc}$ = semiconductor space charge complex impedance, $\Omega\cdot$m$^2$
$\tilde{Z}_H$ = Helmholtz complex impedance, $\Omega\cdot$m$^2$

### *Greek letters*

$\epsilon$ = semiconductor permittivity, F/m
$\epsilon_0$ = vacuum permittivity, $8.85\times10^{-12}$ F/m
$\rho^+$ = positive space charge density, C$\cdot$m$^{-3}$
$\rho_L$ = contribution to the space charge density from the localized states, C$\cdot$m$^{-3}$
$\tau$ = time constant for capture-emission processes, s
$\varphi_m$ = phase angle of the measured complex admittance, rad
$\psi_s$ = total band bending, V
$\psi_c$ = band bending at $x_c$, V
$\omega$ = angular frequency, s$^{-1}$

## Literature Cited


Abram, R. A., and P. J. Doherty, "A Theory of Capacitance-Voltage Measurements on Amorphous Silicon Schottky Barriers," *Phil. Mag. B*, **45**, 167 (1982).

Archibald, I.W., and R. A. Abram, "A Theory of the Admittance of an Amorphous Silicon Schottky Barrier," *Phil. Mag. B*, **48**, 111 (1983).

Archibald, I. W., and R. A. Abram, "More Theory of the Admittance of an Amorphous Silicon Schottky Barrier," *Phil. Mag. B*, **54**, 421 (1986).

Bonham, D. B., and M. E. Orazem, "A Mathematical Model for the AC Impedance of Semiconducting Electrodes," *AIChE J.*, **34**, 465 (1988).

Burleigh, T. D., "Anodic Photocurrents and Corrosion Currents on Passive and Active-Passive Metals," *Corrosion (NACE)*, **45**, 464 (1989).

Cohen, J. D., and D. V. Lang, "Calculation of the Dynamic Response of Schottky Barriers with a Continuous Distribution of Gap States," *Phys. Rev. B*, **25**, 5321 (1982).

Cohen, M. H., H. Fritzsche, and S. R. Ovshinsky, "Simple Band Model for Amorphous Semiconducting Alloys," *Phys. Rev. Lett.*, **22**, 1065 (1969).

Dean, M. H., and U. Stimming, "Capacity of Semiconductor Electrodes with Multiple Bulk Electronic States: 2. Applications to Amorphous Semiconductor Electrodes," *J. Phys. Chem.*, **93**, 8053 (1989).

Di Quarto, F., A. Di Paola, and C. Sunseri, "Kinetics of Growth of Amorphous $WO_3$ Anodic Films on Tungsten," *J. Electrochem. Soc.*, **127**, 1016 (1980).

Di Quarto, F., S. Piazza, and C. Sunseri, "Amorphous Semiconductor/Electrolyte Junction: a New Interpretation of the Impedance Data of Amorphous Semiconducting Films on Metals," *Ber. Bunsenges. Phys. Chem.*, **90**, 549 (1986).

Di Quarto, F., S. Piazza, and C. Sunseri, "Amorphous Semiconductor/Electrolyte Junctions: Photoelectrochemical Behaviour of Thin $Nb_2O_5$ Anodic Films," *Ber. Bunsenges. Phys. Chem.*, **91**, 437 (1987a).

Di Quarto, F., S. Piazza, R. D'Agostino, and C. Sunseri, "Amorphous Semiconductor-Electrolyte Junction: Influence of Wavelength and Oxide Thickness on the Photocharacteristics of a-$Nb_2O_5$ Anodic Films," *J. Electroanal. Chem.*, **228**, 119 (1987b).

Di Quarto, F., S. Piazza, and C. Sunseri, "Amorphous Semiconductor/Electrolyte Junction: Impedance Study on the a-$Nb_2O_5$-Electrolyte Junction," *Electrochim. Acta*, **35**, 99 (1990).

Di Quarto, F., V. O. Aimiuwu, S. Piazza, and C. Sunseri, "Amorphous Semiconductor-Electrolyte Junction: Energetics at the a-$WO_3$/Electrolyte Junction," *Electrochim. Acta*, **36**, 1817 (1991).

Fonash, S. J., "A Reevaluation of the Meaning of Capacitance Plots for Schottky-Barrier-Type Diodes," *J. Appl. Phys.*, **54**, 1966 (1983).

Gerischer, H., "Solar Photoelectrolysis with Semiconductor Electrodes," *Topics in Applied Physics: Solar Energy Conversion*, Vol. 31, p. 115, B. O. Seraphin, ed., Springer Verlag, Berlin (1979).

Gerischer, H., "The Impact of Semiconductors on the Concepts of Electrochemistry," *Electrochim. Acta*, **35**, 1677 (1990).

Gomes, W. P., and F. Cardon, "Electron Energy Levels in Semiconductor Electrochemistry," *Progress in Surface Science*, Vol. 12, p. 155, Pergamon Press (1982).

Heller, A., "Electrochemical Solar Cells," *Solar Energy*, **29**, 153 (1982).

Losee, D. L., "Admittance, Spectroscopy of Impurity Levels in Schottky Barriers," *J. Appl. Phys.*, **46**, 2204 (1975).

Mott, N.F., and E. A. Davis, *Electronic Processes in Noncrystalline Materials*, 2nd ed., Clarendon Press, Oxford (1979).

Pleskov, Yu. V., and Yu. Ya. Gurevich, *Semiconductor Photoelectrochemistry*, Chap. 3, Consultants Bureau, New York (1986).

Roberts, G. I., and C. R. Crowell, "Capacitance Energy Level Spectroscopy of Deep-Lying Semiconductor Impurities Using Schottky Barriers," *J. Appl. Phys.*, **41**, 1767 (1970).

Sato, N., "Toward a More Fundamental Understanding of Corrosion Processes," *Corrosion (NACE)*, **45**, 354 (1989).

Snell, A. J., K. D. Mackenzie, P. G. Le Comber, and W. E. Spear, "The Metal-Amorphous Silicon Barrier, Interpretation of Capacitance and Conductance Measurements," *J. of Non-Crystalline Solids*, **35-36**, 593 (1980).

Spear, W. E., and S. H. Baker, "Electronic Properties of Metal-Amorphous Silicon Barriers and Junctions," *Electrochim. Acta*, **34**, 1691 (1989).

Stimming, U., "Photoelectrochemical Studies of Passive Films," *Electrochim. Acta*, **31**, 415 (1986).

*Manuscript received Apr. 5, 1991, and revision received Nov. 27, 1991.*